Novel Single-Phase PWM AC–AC Converters Solving Commutation Problem Using Switching Cell Structure and Coupled Inductor

Hyun-Hak Shin, Honnyong Cha, *Member, IEEE*, Heung-Geun Kim, *Senior Member, IEEE*, and Dong-Wook Yoo, *Member, IEEE*

***Abstract*—This paper presents novel single-phase pulse width modulation (PWM) ac–ac converters that can solve the commutation problem in single-phase direct PWM ac–ac converters without sensing the input voltage polarity. By using a basic switching cell structure and coupled inductors, the proposed ac–ac converters can be short- and open-circuited without damaging the switching devices. Neither lossy RC snubber nor dedicated soft commutation strategy is required in the proposed converter. By replacing the conventional phase-leg of the PWM ac–ac converters with the switching cell structure and the coupled inductor, three novel buck, boost, and buck-boost type PWM ac–ac converters are developed. Although two coupled inductors are required for the proposed converter, the input inductor of the proposed converter can be much smaller than that of the conventional PWM ac–ac converters. The volume of the magnetic components can be further reduced by increasing switching frequency of the converter because very fast recovery diodes can be selected externally. In order to verify performance and robustness of the proposed converter, a 200-W boost type prototype converter was built and tested with both mismatched gate signals and highly distorted input voltage.**

***Index Terms*—AC–AC converter, commutation problem, coupled inductor, pulse width modulation (PWM), switching cell.**

I. Introduction

FOR AC–AC power conversion, the conventional approach is to use a diode or PWM rectifier followed by a PWM voltage-source inverter with a DC link. Other approaches include phase-controlled ac–ac converters employing thyristors, matrix converters, and so on. The output voltage and frequency can be varied with these structures. However, for applications where only voltage regulation is required, direct PWM ac–ac converters are a more practical choice in terms of cost and size [1]. Fig. 1 shows the basic single-phase direct PWM ac–ac converters or ac–ac choppers [2].

Manuscript received December 20, 2013; revised March 1, 2014 and April 29, 2014; accepted May 29, 2014. Date of publication June 12, 2014; date of current version November 3, 2014. This work was supported by the Basic Science Research Program through the National Research Foundation of Korea funded by the Ministry of Science, ICT, and future Planning under Grant NRF-2013R1A2A2A01069038. Recommended for publication by Associate Editor J. R. Espinoza.

H.-H. Shin and H. Cha are with the School of Energy Engineering, Kyungpook National University, 1370 Daegu, Korea (e-mail: night1483@knu.ac.kr; chahonny@knu.ac.kr).

H.-G. Kim is with the Department of Electrical Engineering, Kyungpook National University, 1370 Daegu, Korea (e-mail: hgkim@knu.ac.kr).

D.-W. Yoo is with the Korea Electrotechnology Research Institute, 642-120 Changwon, Korea (e-mail: dwyoo@keri.re.kr.)

Color versions of one or more of the figures in this paper are available online at http://ieeexplore.ieee.org.

Digital Object Identifier 10.1109/TPEL.2014.2330351

The ac–ac circuits shown in Fig. 1 have a common commutation problem. For example, for the buck-type converter shown in Fig. 1(a), the switches S_2 and S_3 are both turned ON and OFF simultaneously, and they are complementary to the switches S_1 and S_4 in an ideal case. However, due to the different time delays and limited switching speed of the switching devices, there inherently exists a short dead-time or an overlap-time between switches. During the dead-time, there is no current path for the output filter inductor (L_o), so the switches may be damaged by excessive voltage. Similarly, the switches may be damaged by excessive current when there is an overlap-time between switches S_1 and S_2 (or S_3 and S_4), because the input voltage will be short-circuited. Fig. 2 illustrates this problem.

In order to solve this, bulky and lossy RC snubber circuits are required to protect the switches. A better way is to implement safe commutation strategies that provide smooth current transition. Several soft commutation strategies have been introduced and employed successfully in the circuits shown in Fig. 1 [2]. However, most of them solve the commutation problem by sensing the voltage or current polarity of the converter. When the voltage or current is distorted significantly, especially around the zero crossing point, the conventional methods still cannot provide completely safe and reliable commutation.

In this paper, very robust single-phase PWM ac–ac converters without the commutation problem are introduced. The proposed converters use basic switching cell structure and coupled inductors to implement phase legs of the converter. With this structure, the proposed converters can tolerate both dead-time and overlap-time without damaging switching devices. In addition, the proposed converters do not need to sense the voltage or current polarity for commutation. Therefore, highly robust and reliable PWM ac–ac converters can be developed. A 200-W prototype ac–ac converter was built and tested to verify the performance of the proposed idea.

II. Switching-Cell Structure and the Proposed Single-Phase PWM AC–AC Converters

The switching cell structures have been introduced in several previous studies, and the two basic switching cells are shown in Fig. 3 [3]–[20]. These switching cells are commonly called P-cell and N-cell. Each cell is composed of one switching device and one diode connected in series. The center terminal between the switching device and the diode is generally connected to a current source or inductor [3]–[5].

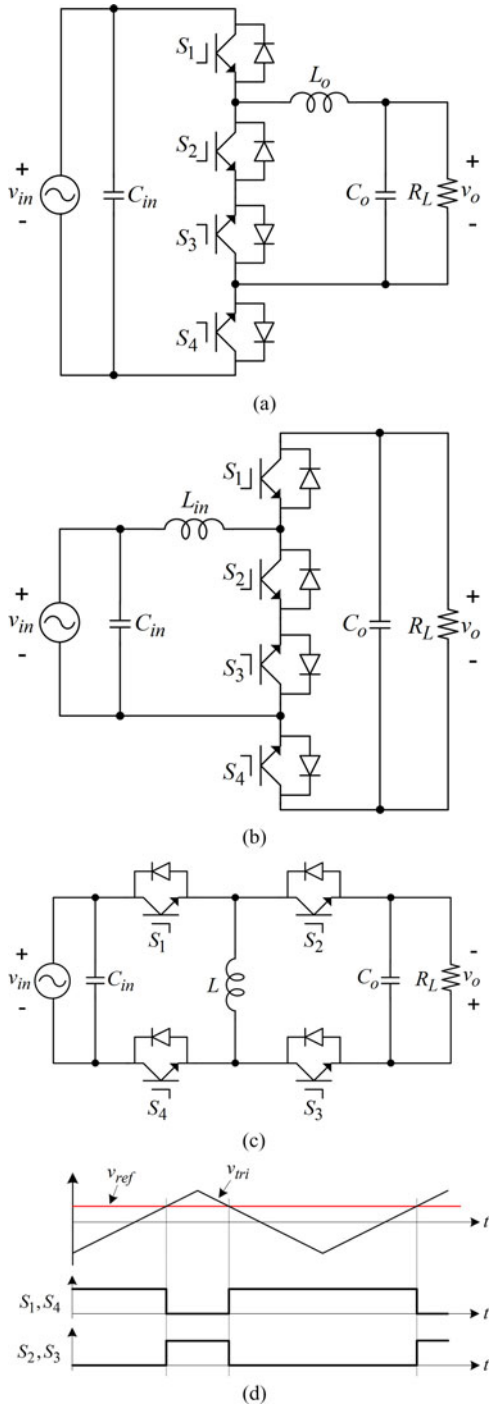

Fig. 1. Conventional single-phase direct PWM ac–ac converters and ideal gate signals. (a) Buck type. (b) Boost type. (c) Buck-boost type. (d) Gate signals (ideal).

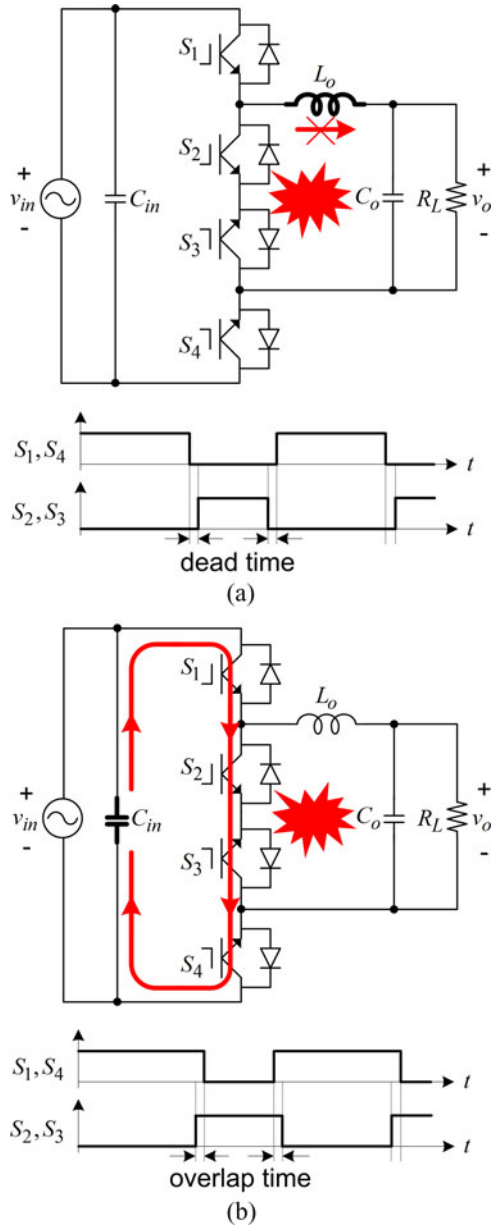

Fig. 2. Commutation problem in conventional PWM ac–ac converters.

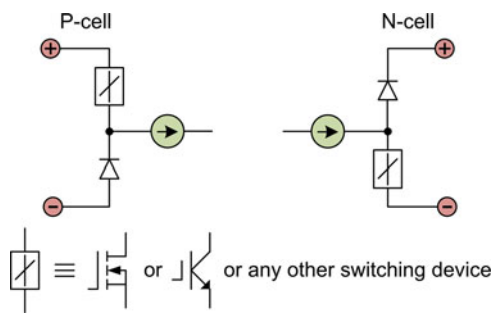

Fig. 3. Basic switching cell [3]–[5].

Fig. 4 compares phase-leg implementations. When compared with the conventional phase-leg, the switching cell structure is slightly different. Since a current source or inductor is generally connected to the common junction of the switching cell, this structure can avoid the shoot-through problem caused by issues such as mis-triggering of the gate signals. Thus, a highly reliable and robust converter system can be designed. Furthermore, very fast recovery diodes can be selected for the diodes D_T and

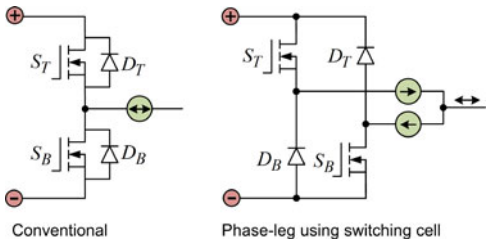

Fig. 4. Phase-leg implementation [3]–[5].

D_B because they are selected externally, which leads to high frequency operation of converter system. As a result, the size of the magnetic components can be reduced significantly [13].

Fig. 5 shows the proposed single-phase buck, boost, and buck-boost type PWM ac–ac converters. Compared with the conventional PWM ac–ac converters shown in Fig. 1, the proposed converters use the basic switching cell structure shown in Fig. 4 to form a phase-leg.

The top leg consists of two switches (S_1,S_2), two diodes (D_1,D_2), a coupled inductor (CL_1), and a capacitor (C_1). The same symmetric structure can be made for the bottom leg. The two capacitors C_1 and C_2 are added across each phase-leg to provide a current path when S_1 and S_2 (or S_3 and S_4) are both turned OFF. These capacitors serve as the input or output filter capacitors. Moreover, they also serve as a simple snubber capacitor that can further suppress the switch voltage overshoot caused by the stray inductances of the circuit. In this paper, the boost type ac–ac converter is considered, although the buck and buck-boost type can be analyzed similarly.

Fig. 6 shows the modulation scheme of the proposed ac–ac converters. The two 180° out of phase triangular waves ($v_{\mathrm{tri.1}}$ and $v_{\mathrm{tri.2}}$) are compared with a reference voltage (v_{ref}) to generate PWM gate signals. Note that S_2 and S_3 take the inverse of the signals generated by $v_{\mathrm{tri.2}}$ and v_{ref}.

III. Operation of the Proposed AC–AC Converters

Fig. 7 shows the operation of the proposed converter with current flowing between the switch legs and the coupled inductors. The positive half cycle of the input voltage is only considered, but the negative half cycle can be analyzed in the same manner. Due to the symmetric structure between the top and bottom leg, the midpoint between the top and bottom leg is defined as a ground potential in this paper and the connection terminals of each coupled inductor are labeled as "*A*" and "*B*" (see Fig. 7).

Fig. 8 shows the key operational waveforms of the proposed converter when D $<$ 0.5. From Fig. 8, the converter can be described as having four continuous conduction modes and a three-level unipolar voltage (v_{C_1},$v_{C_1}/2$, 0 for the top-leg and v_{C_2}, $v_{C_2}/2$, 0 for the bottom-leg) is generated at points "*A*" and "*B*" depending on the duty cycle of the converter during one fundamental frequency (60 Hz), respectively (see Fig. 10).

Fig. 9 shows the current ripple analysis of the input inductor and the coupled inductors. As illustrated in Fig. 9, there are two distinct current components: the common-mode (or circulating) current (i_{cm1} and i_{cm2}) and the input inductor current

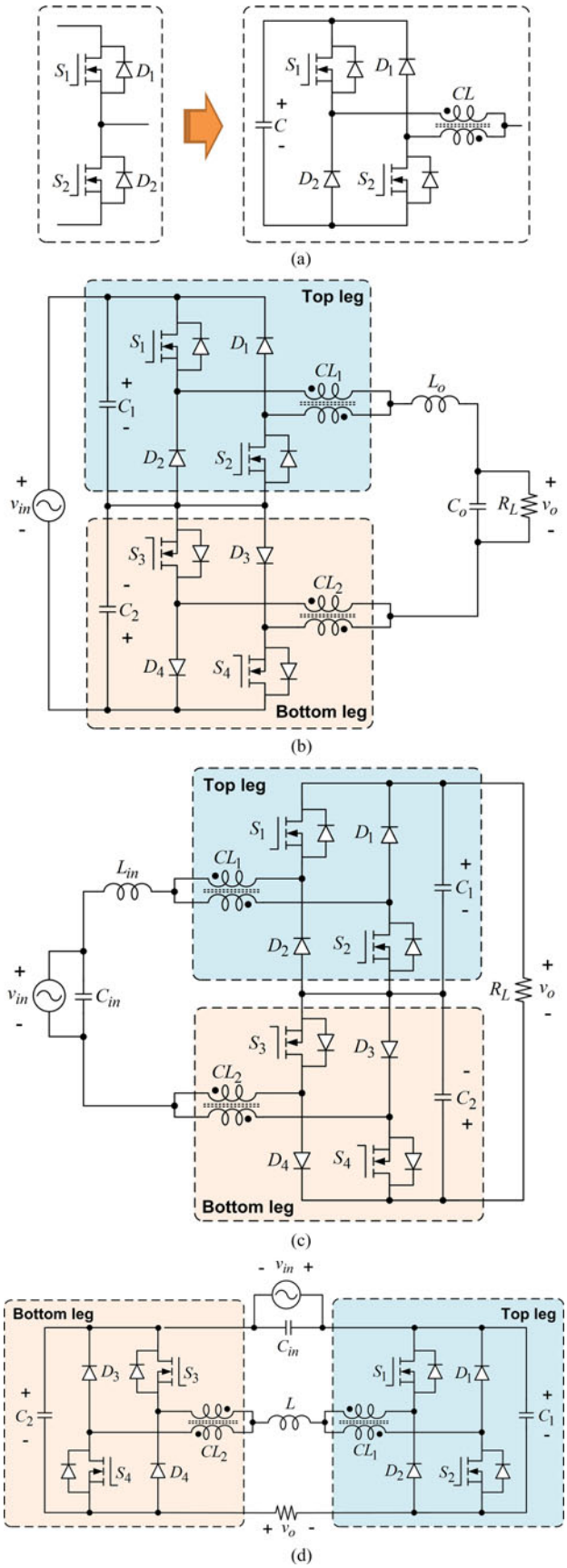

Fig. 5. Proposed single-phase PWM ac–ac converters. (a) Switching cell with coupled inductor. (b) Buck type. (c) Boost type. (d) Buck-boost type.

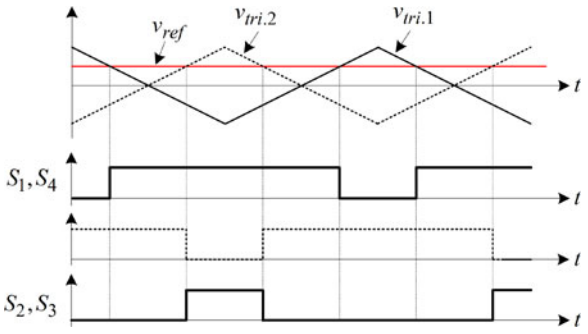

Fig. 6. Gate signal generation of the proposed ac–ac converters.

($i_{L_{\rm in}}$). The common-mode currents are the average of the winding currents ($i_{L_1} - i_{L_4}$), and the input inductor current is the difference between the winding currents [7]. Thus, the following relationships always apply regardless of the operation modes:

$$i_{\rm cm1} = \frac{i_{L_1} + i_{L_2}}{2} \tag{1}$$

$$i_{\rm cm2} = \frac{i_{L_3} + i_{L_4}}{2} \tag{2}$$

$$i_{L_{\rm in}} = i_{L_2} - i_{L_1} = i_{L_4} - i_{L_3} \tag{3}$$

$$v_o = v_{C_1} - v_{C_2}. \tag{4}$$

In the analysis, the two coupled inductors are assumed to be identical to each other and the coupling coefficient is assumed to be close to unity (tight coupling). The following is a detailed mode analysis of the proposed converter. As shown in Fig. 8, D is defined as the time interval when S_2 and S_3 are on during one switching period T_s.

A. Mode 1 [$0 \sim DT_s$]

In this mode, the switches $S_1 - S_4$ are all turned ON, and the diodes $D_1 - D_4$ are all turned OFF. The input energy is stored in the $L_{\rm in}$. The voltage and current relationships are as follows:

$$v_A = \frac{v_{C_1}}{2}, \quad v_B = \frac{v_{C_2}}{2} \tag{5}$$

$$v_{AB} = v_A - v_B = \left(\frac{v_{C_1}}{2} - \frac{v_{C_2}}{2}\right) = \frac{v_o}{2} \tag{6}$$

$$v_{L_{\rm in}} = v_{\rm in} - v_{AB} = v_{\rm in} - \frac{v_o}{2} \tag{7}$$

$$\frac{di_{L_{\rm in}}}{dt} = \frac{v_{L_{\rm in}}}{L_{\rm in}} = \frac{v_{\rm in} - v_o/2}{L_{\rm in}} \tag{8}$$

$$\frac{di_{\rm cm1}}{dt} = \frac{v_{C_1}}{4L_s} \tag{9}$$

$$\frac{di_{\rm cm2}}{dt} = \frac{v_{C_2}}{4L_s} \tag{10}$$

where L_s is self-inductance of the coupled inductor.

B. Mode 2 [$DT_s \sim 0.5T_s$]

The switches S_2 and S_3 are turned OFF, while S_1 and S_4 remain ON. The diodes D_1 and D_4 are turned ON due to freewheeling action and D_2 and D_3 remain OFF. The stored energy in the $L_{\rm in}$ is transferred to the output through D_1 and S_4. The voltage and current relationships are as follows:

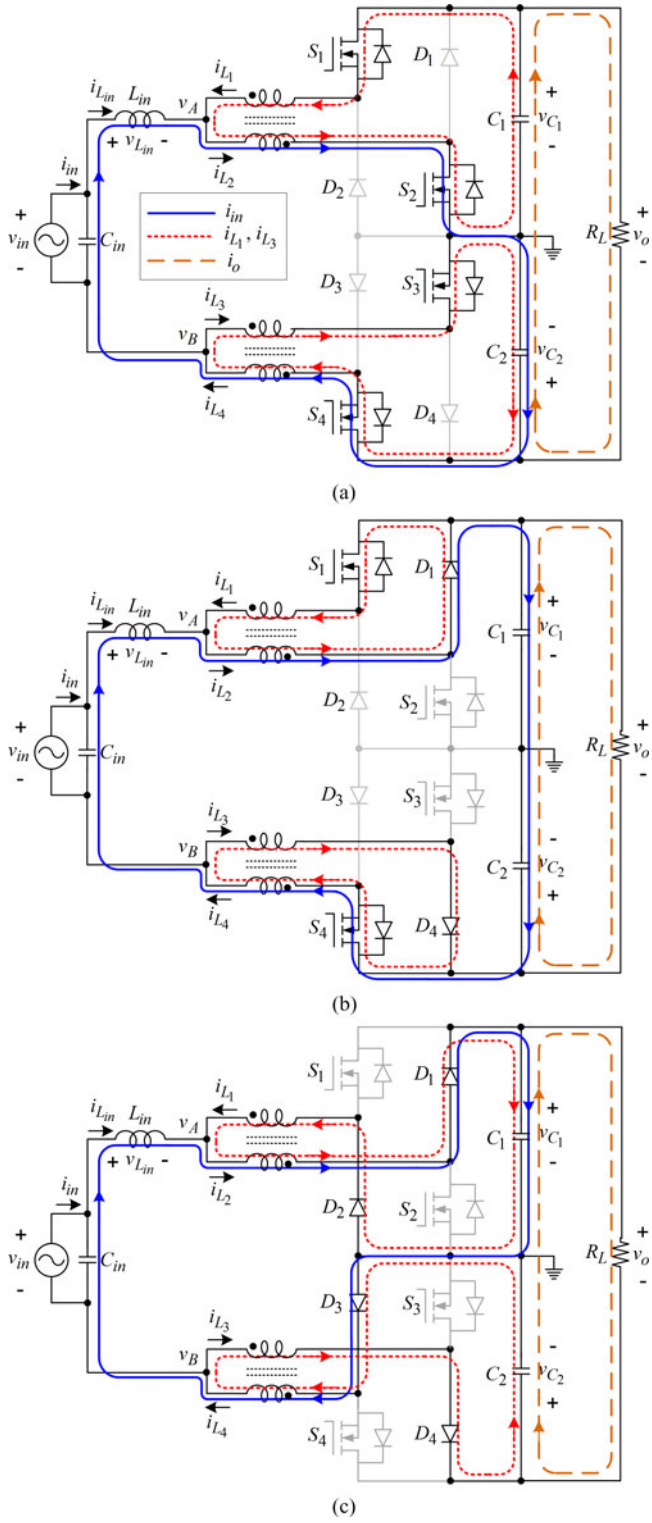

Fig. 7. Operational modes of the proposed converter (D < 0.5). (a) Mode 1. (b) Mode 2 and 4. (c) Mode 3.

$$v_A = v_{C_1}, \quad v_B = v_{C_2} \tag{11}$$

$$v_{AB} = v_A - v_B = v_{C_1} - v_{C_2} = v_o \tag{12}$$

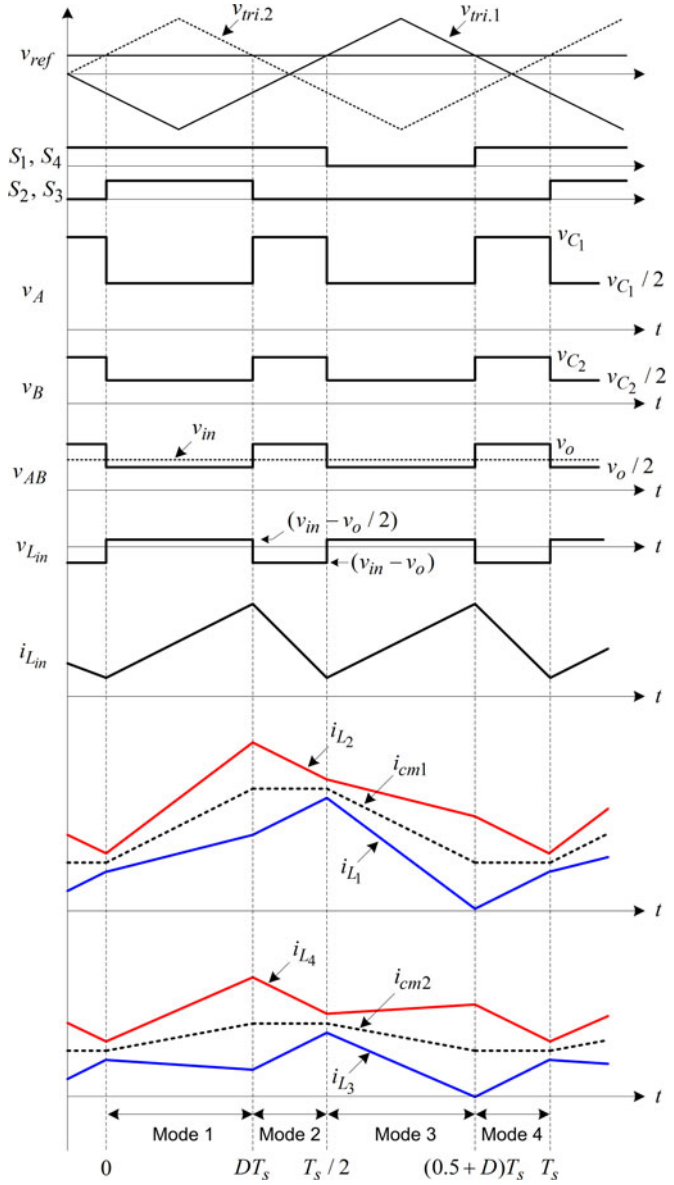

Fig. 8. Key operational waveforms of the proposed single-phase PWM boost ac–ac converter when D < 0.5.

$$v_{L_{\rm in}} = v_{\rm in} - v_{AB} = v_{\rm in} - v_o \tag{13}$$

$$\frac{di_{L_{\rm in}}}{dt} = \frac{v_{L_{\rm in}}}{L_{\rm in}} = \frac{v_{\rm in} - v_o}{L_{\rm in}} \tag{14}$$

$$\frac{di_{\rm cm1}}{dt} = \frac{di_{\rm cm2}}{dt} = 0. \tag{15}$$

C. Mode 3 $[0.5T_s \sim (0.5+D)T_s]$

Mode 3 is similar to mode 1, except that the switches $S_1 - S_4$ are all turned OFF, and $D_1 - D_4$ are all turned ON. Again, the input energy is stored in the $L_{\rm in}$. The voltages v_A, v_B, v_{AB}, and $v_{L_{\rm in}}$ are the same as in mode 1. The common mode currents are as follows:

$$\frac{di_{\rm cm1}}{dt} = -\frac{v_{C_1}}{4L_s} \tag{16}$$

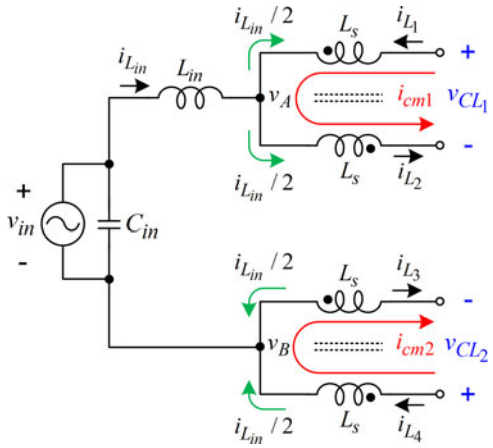

Fig. 9. Common mode and input inductor current.

$$\frac{di_{\rm cm2}}{dt} = -\frac{v_{C_2}}{4L_s}. \tag{17}$$

D. Mode 4 $[(0.5+D)T_s \sim T_s]$

The operation of mode 4 is exactly the same as that of mode 2.

A similar analysis can be conducted when D > 0.5. The only difference is that v_A and v_B become zero instead of v_{C_1} and v_{C_2} during modes 2 and 4. Thus, all the inductor voltage and current waveforms are changed accordingly. Fig. 10 illustrates this.

From the volt-sec (or flux) balance condition on the $L_{\rm in}$, voltage gain of the proposed boost type ac–ac converter can be calculated as

$$\frac{v_o}{v_{\rm in}} = \frac{1}{1-D}. \tag{18}$$

From (18), voltage gain of the proposed boost type ac–ac converter is exactly the same as those of the conventional boost DC-DC converter and the boost type PWM ac–ac converter.

IV. Ripple Current Analysis of the Coupled Inductor and Input Inductor

In this section, the current ripple of the input inductor and the two coupled inductors are investigated. From the input inductor current ($i_{L_{\rm in}}$) waveform in Fig. 8, one can notice that $L_{\rm in}$ in the proposed converter can be made much smaller than the input inductor in the conventional boost type ac–ac converter shown in Fig. 1(b) because the $L_{\rm in}$ in the proposed converter experiences twice the switching frequency and less voltage is applied across the $L_{\rm in}$. From (1)–(3), the currents in the coupled inductor can be calculated if the common mode and the input inductor current are known.

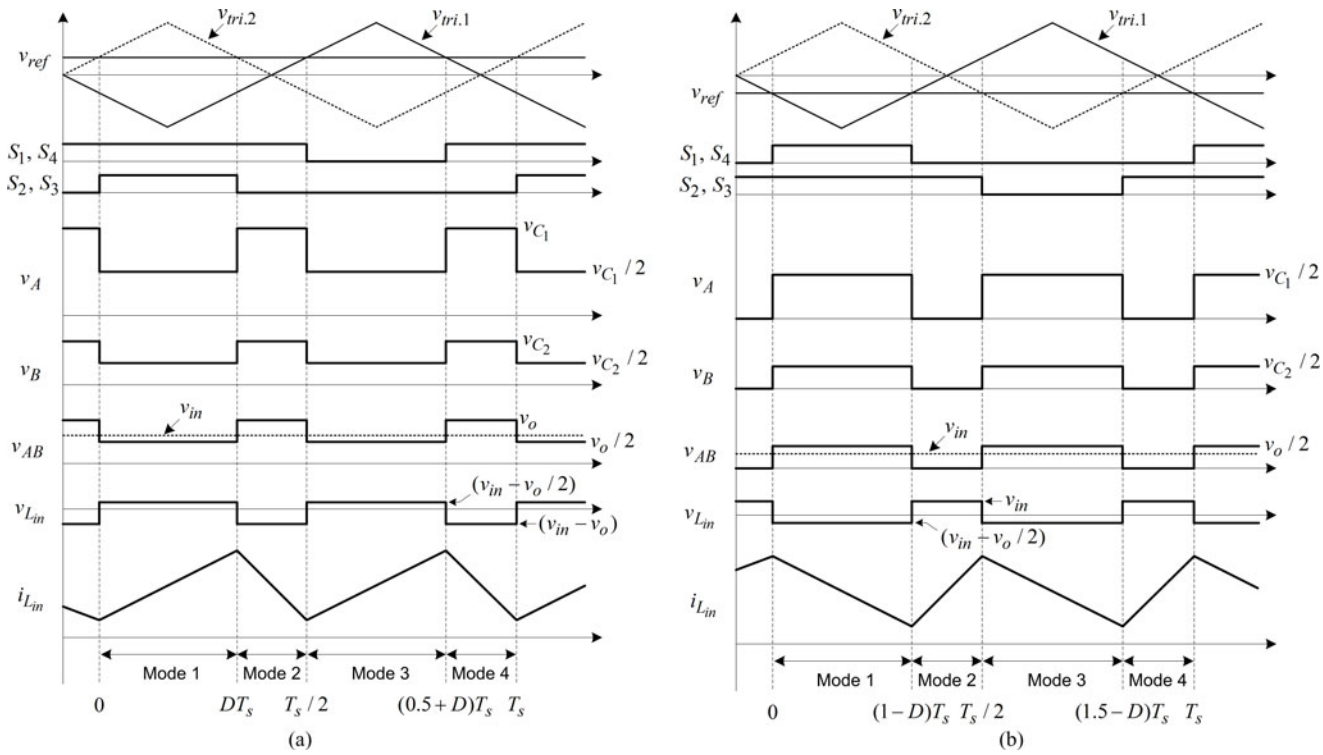

Fig. 10. Comparison of key waveforms. (a) D < 0.5. (b) D > 0.5.

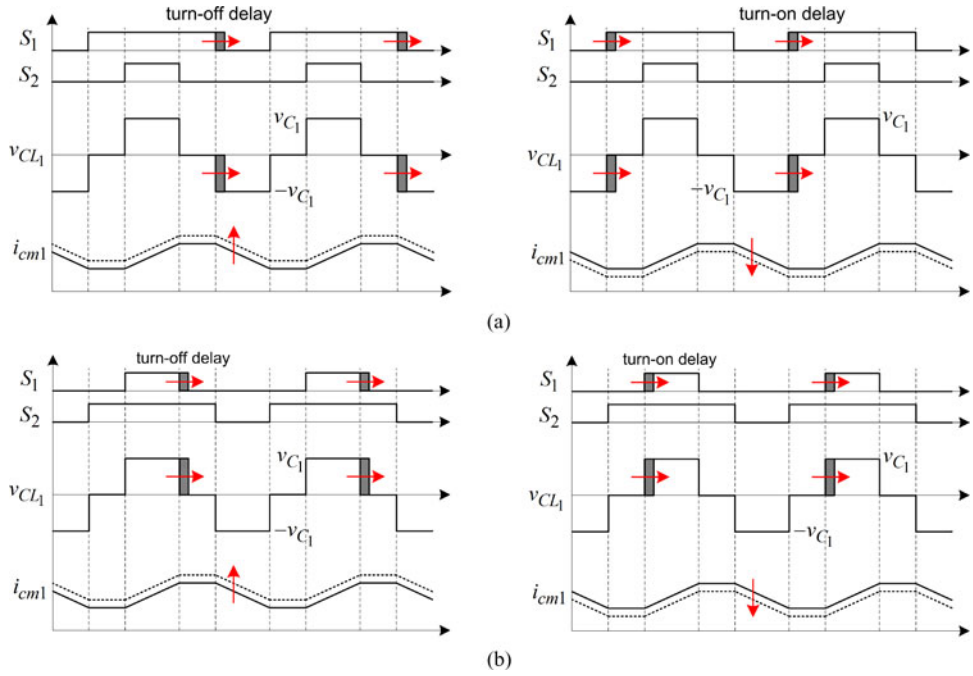

Fig. 11. Effect of switch turn-on and turn-off delays on the common-mode dc current component. (a) When D < 0.5. (b) When D > 0.5.

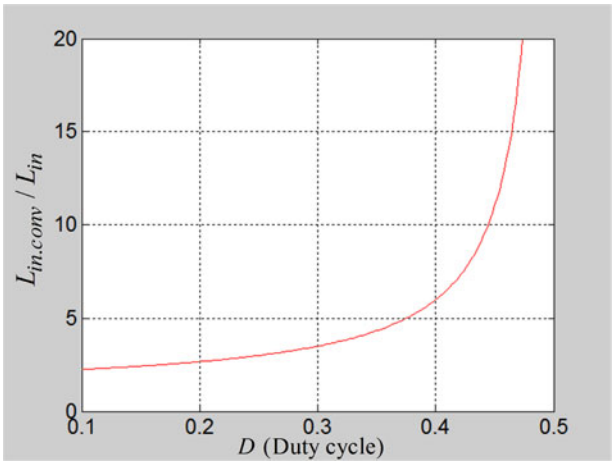

Fig. 12. Comparison of input inductance value.

TABLE I
ELECTRICAL SPECIFICATIONS

Input voltage range	110–220 Vrms/60 Hz	
Output voltage	220 Vrms/60 Hz	
Output power	200 W	
Switching frequency	50 kHz	
MOSFET ($S_1 - S_4$)	47N60CFD	
Diode ($D_1 - D_4$)	RHRG3060	
$C_{\rm in}$, C_1, C_2	2.2 μF	
Input inductor ($L_{\rm in}$)	Core	PQ2620
	No. of turns	21 T
	Inductance	100 μH
Coupled inductors (CL_1, CL_2)	Core	PQ3230
	No. of turns	37 T
	Self inductance (L_s)	200 μH

A. Input Inductor Design

The current ripple in the $L_{\rm in}$ can be calculated from (8) and (18) as follows:

$$\Delta i_{L_{\rm in}} = \frac{(0.5 - D)D}{L_{\rm in}} v_o T_s. \tag{19}$$

Thus, the maximum current ripple in the $L_{\rm in}$ occurs when $D = 0.25$ with $v_o = v_{o.\max}$. In (19), T_s is the switching period of the converter ($T_s = 1/f_{sw}$).

B. Coupled Inductor Design

As mentioned in Section III, the coupled inductors are assumed to have perfect coupling. From (9) and (10), the current ripple of the common mode currents are calculated as

$$\Delta i_{cm1} = \frac{v_{C_1}}{4L_s} DT_s \tag{20}$$

$$\Delta i_{cm2} = \frac{v_{C_2}}{4L_s} DT_s. \tag{21}$$

From (1)–(3) and Fig. 9, the winding currents of the coupled inductors can be rewritten as

$$i_{L_1} = i_{cm1} - \frac{i_{L_{\rm in}}}{2} \tag{22}$$

$$i_{L_2} = i_{\rm cm1} + \frac{i_{L_{\rm in}}}{2} \tag{23}$$

$$i_{L_3} = i_{\rm cm2} - \frac{i_{L_{\rm in}}}{2} \tag{24}$$

$$i_{L_4} = i_{\rm cm2} + \frac{i_{L_{\rm in}}}{2}. \tag{25}$$

From (19)–(25), the current ripple equations of the coupled inductors can be derived in each mode, and the maximum winding current ripple occurs when either v_{C_1} or v_{C_2} is zero, which are expressed as

$$\Delta i_{L_{x.\max}} = \left(\frac{1}{L_s} + \frac{1 - 2D}{L_{\rm in}}\right) \frac{v_o}{4} DT_s, \quad x = 1, 2, 3, 4. \tag{26}$$

From (26), current ripple of the coupled inductors can be reduced with large L_s. However, the coupled inductors should have an airgap in the core due to the switching cell structure. The existence of the airgap will reduce L_s. In addition to this, it should be noted that the switch turn-off and turn-on delays have effect on the common-mode dc current component ($i_{\rm cm1}$,$i_{\rm cm2}$) and finally on the saturation of the coupled inductor. Fig. 11 shows the effect of switch delay on the $i_{\rm cm1}$. As shown in Fig. 11(a), switch turn-off delay will produce positive voltage drop across the coupled inductor (v_{CL_1}, see the label in Fig. 9) and set up the dc offset (i.e., increases $i_{\rm cm1}$) and leads to core saturation, whereas switch turn-on delay will produce negative voltage drop across the coupled inductor (v_{CL_1}) and negate the dc offset (i.e., decreases $i_{\rm cm1}$) and does not cause core saturation. Moreover, device voltage drops in the MOSFETs and diodes can also negate the dc offset [7], [8]. Fig. 11(b) shows the same effect when D $>$ 0.5. Therefore, small difference between S_1 and S_2 (or S_3 and S_4) to have negative voltage drop across the coupled inductors can solve the saturation problem [8]. Experimental waveforms in later section will verify this.

Although, the two coupled inductors make the proposed converter less attractive, the input inductor ($L_{\rm in}$) of the proposed converter experiences twice of the switching frequency and the voltage across the $L_{\rm in}$ becomes half when compared with that of the conventional boost type ac–ac converter shown in Fig. 1(b). Therefore, the $L_{\rm in}$of the proposed converter can be much smaller than that of the conventional converter. The equation for the current ripple of the input inductor is expressed in (19). The equation for the current ripple of the input inductor with conventional PWM ac–ac converter ($L_{\rm in.conv}$) is expressed as follows:

$$\Delta i_{L_{\rm in.conv}} = \frac{(1 - D)D}{L_{\rm in.conv}} v_o T_s. \tag{27}$$

Thus, maximum current ripple in $L_{\rm in.conv}$ occurs when $D =$ 0.5 with $v_o = v_{o.\max}$. Fig. 12 shows the required inductance of the conventional ac–ac converter to maintain same input inductor current ripple as the proposed converter when D varies from 0.1 to 0.5.

As shown, the required input inductance of the conventional ac–ac converter ($L_{\rm in.conv}$) is much greater than that of the proposed converter. For example, the $L_{\rm in.conv}$ is almost 11 times of $L_{\rm in}$ when $D = 0.45$. Therefore, the overall volume of the

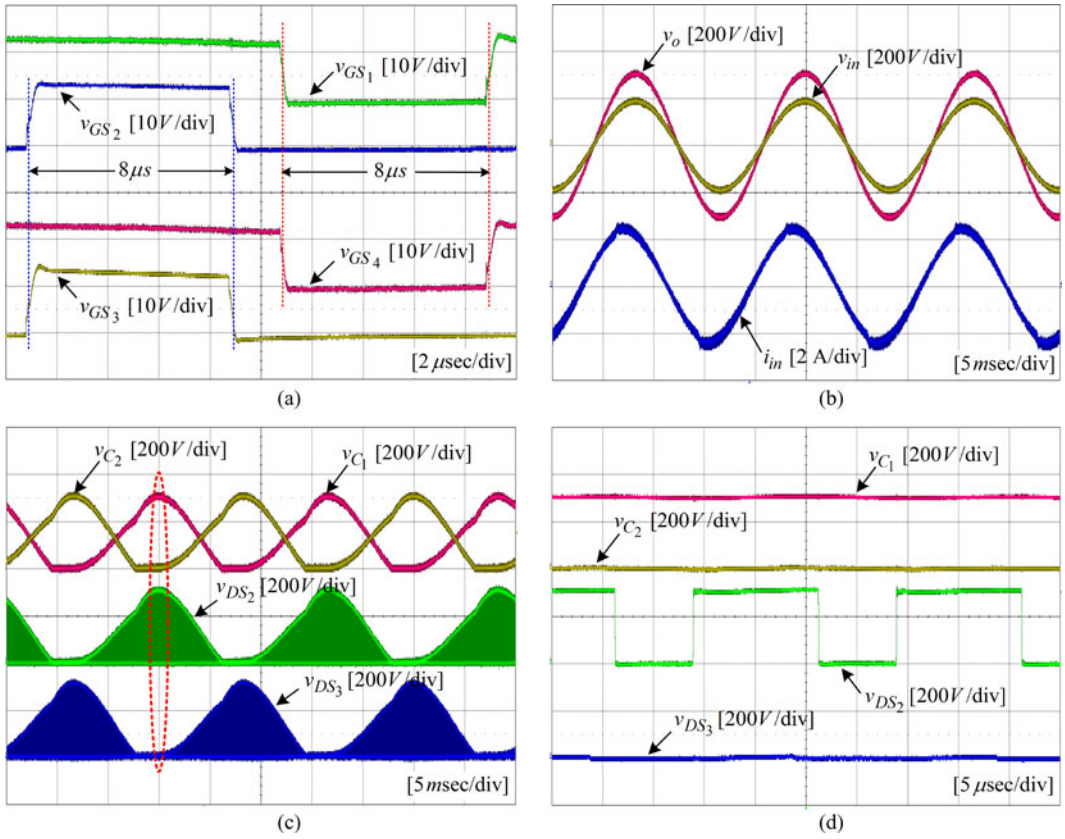

Fig. 13. Experimental waveforms of the proposed converter with ideal switching conditions ($V_o = 220Vrms$, $P_o = 200W$, and $D = 0.4$). (a) Gate signals (ideal switching). (d) Magnified waveforms of (c).

magnetic components of the proposed converter will not be much bigger than that of the conventional ac–ac converter. The volume of the magnetic components of the proposed converter can be further reduced with high switching frequency operation of the converter because the diodes in the proposed circuit are selected externally with very fast recovery diodes.

V. Experimental Results

Based on the previous analysis, a boost type 200-W prototype ac–ac converter was built and tested. Table I shows the electrical specifications of the proposed converter. As mentioned in the introduction, the conventional PWM ac–ac converters achieve safe commutation by sensing the input voltage polarity. However, this method still cannot provide reliable commutation especially when the input voltage is highly distorted. The proposed converter does not have such commutation problems. In order to show the robustness of the proposed converter, several experiments were conducted as follows.

Fig. 13 shows the experimental waveforms of the proposed converter with almost ideal switching conditions, where the switching gate signals $S_1 - S_4$ are turned ON and OFF synchronously without any time delay as shown in Fig. 13(a). In this case, there is no commutation problem and the switch drain-source voltages do not have high voltage/current overshoot. Fig. 13(b) shows the input voltage, output voltage, and input current waveforms. Fig. 13(c) shows the voltage waveforms of the output filter capacitors, and the drain-source voltage of switches S_2 and S_3. Fig. 13(d) shows the magnified waveforms of (c).

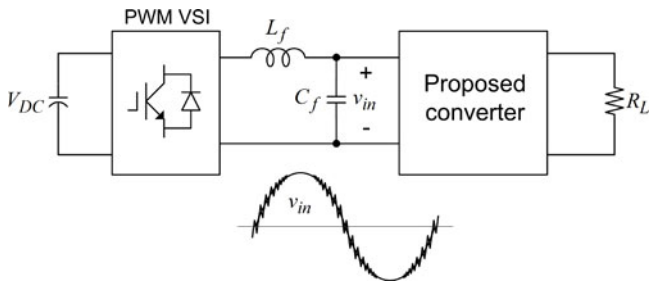

Fig. 14. Test setup to feed a highly distorted ac input voltage to the proposed converter.

In order to prove the robustness of the proposed converter in harsh practical conditions, less than 1-μs time delay was intentionally generated between the switch gate signals. To make things more severe, a highly distorted ac input voltage was fed to the proposed converter. The distorted ac input voltage in this paper was generated from a conventional voltage source inverter built in the laboratory. The test setup is shown in Fig. 14.

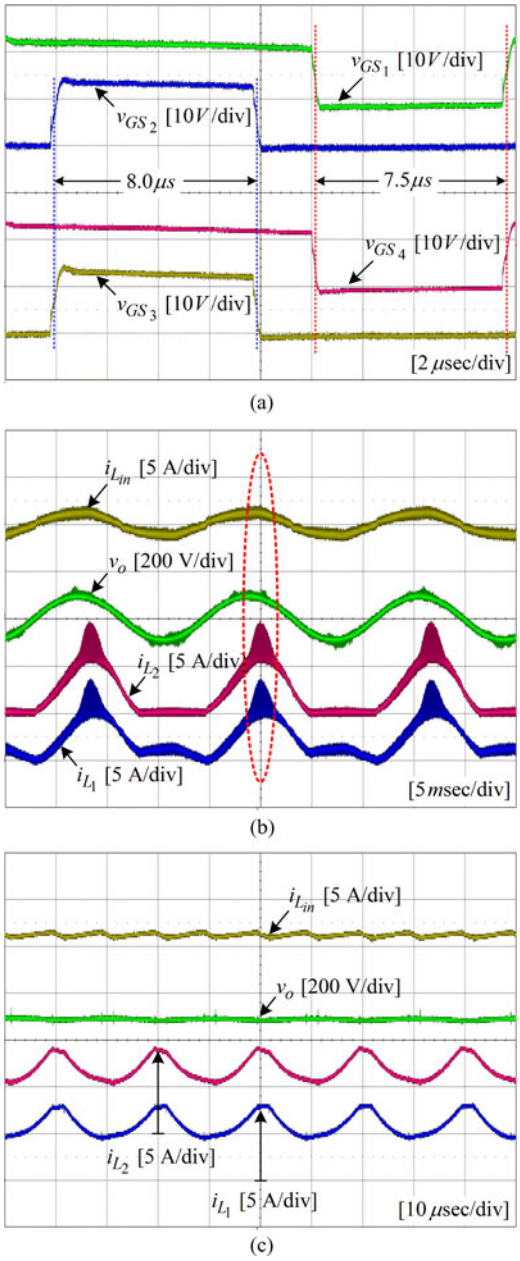

Fig. 15. Experimental waveforms with positive voltage drop across coupled inductor ($V_{in} = 40Vrms$). (a) Gate signals (positive voltage drop). (c) Expanded waveform of (b).

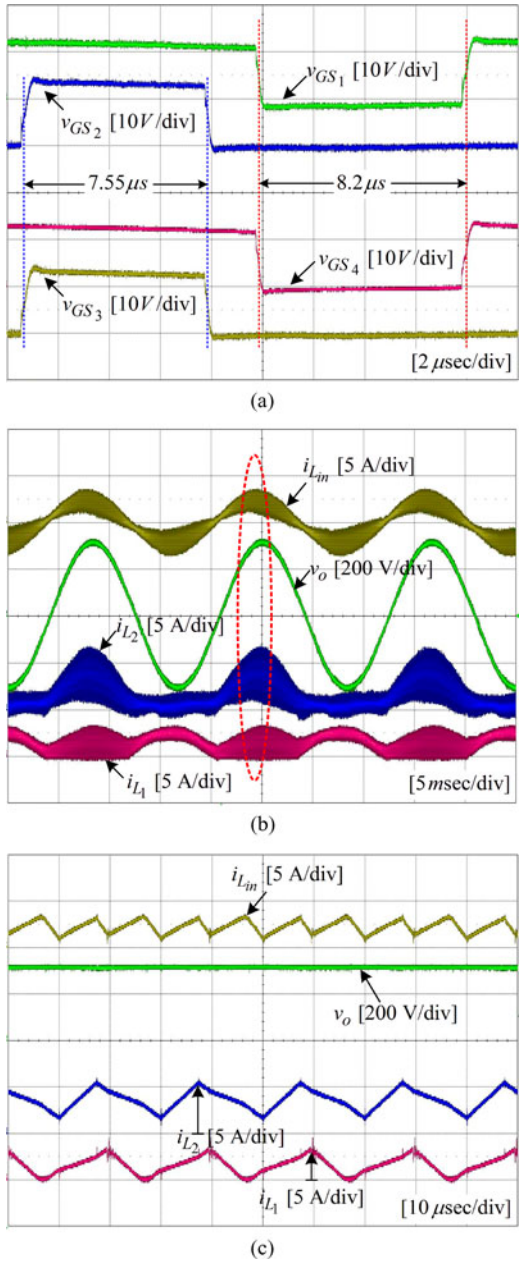

Fig. 16. Experimental waveforms with negative voltage drop across coupled inductor ($V_{in} = 125Vrms$). (a) Gate signals (negative voltage drop). (c) Expanded waveform of (b).

As mentioned in Section IV, positive voltage drop across the coupled inductor will cause core saturation of the coupled inductor. This is verified in Fig. 15. As shown in Fig. 15(a), the switch interval when both S_1 and S_2 are on is 8.0 μs and the interval when both S_1 and S_2 are OFF is 7.5 μs. Fig. 15(b) and (c) show the waveforms. As expected, the coupled inductor saturated even when the input voltage is very small, 40 Vrms.

Fig. 16(a) shows the gate signals to produce negative voltage drop across the coupled inductor. As shown, the switch interval when both S_1 and S_2 are on is 7.55 μs and the interval when both S_1 and S_2 are off is 8.2 μs. Fig. 16(b) and (c) show the waveforms. There is no core saturation even when the input voltage is increased to rated voltage, 125 Vrms.

Further experiments showed that mismatches in S_1 and S_4 (or S_2 and S_3) also do not cause core saturation as long as the gate signals satisfy the negative voltage drop condition.

With these mismatched gate signal and distorted input voltage conditions, huge voltage or current spikes will be generated with the conventional ac–ac converters if proper soft commutation strategies or clamp circuits are not used.

Fig. 17(a) shows the input voltage, output voltage, and switch voltage waveforms. Fig. 17(b) shows the magnified waveforms of (a) around the zero crossing area of the input voltage. With

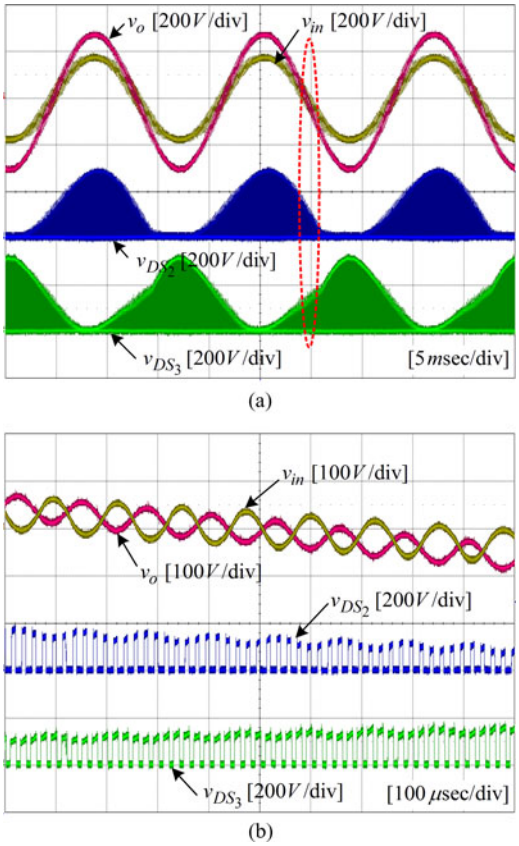

Fig. 17. Experimental waveforms of the proposed converter with mismatched switching and distorted input condition ($V_o = 220Vrms$, $P_o = 200W$, and $D = 0.4$). (b) Magnified waveform of (b).

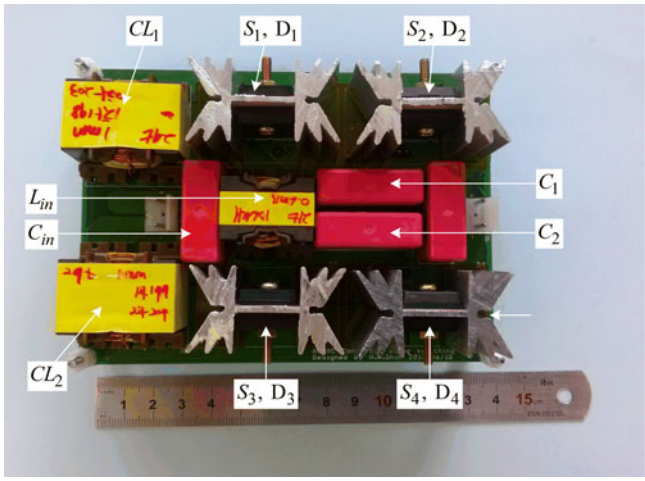

Fig. 18. Prototype picture.

the highly distorted input voltage and mismatched gate signals, the converter still works stably without any additional components and a dedicated safe commutation scheme and there is no noticeable voltage overshoot in the switches.

Fig. 18 shows a picture of the 200-W prototype boost ac–ac converter developed in this paper. Fig. 19 shows the measured

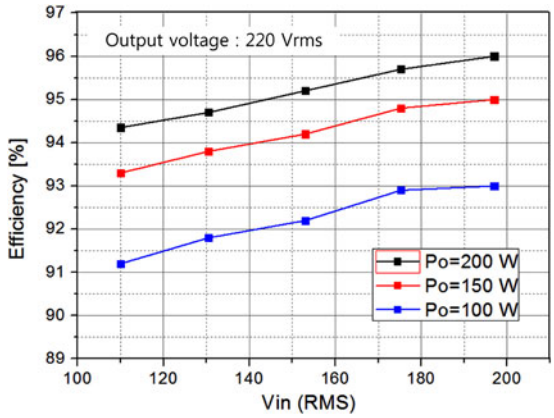

Fig. 19. Measured efficiency.

efficiency of the proposed converter with the input voltage and output power varied.

VI. Conclusion

In this paper, very robust single-phase buck, boost, and buck-boost type PWM ac–ac converters have been proposed. Unlike the existing PWM ac–ac converters, the proposed converters do not need to sense the input voltage polarity for safe commutation and the proposed converter can guarantee stable operation even when the input voltage is highly distorted, which is impossible with the conventional approach. Although two extra coupled inductors are required, the input inductor can be designed to be much smaller than that of the conventional ac–ac converter. The performance of the proposed converter was successfully verified with the 200-W boost type ac–ac converter.

References

[1] F. Z. Peng, C. Lihua, and Z. Fan, "Simple topologies of PWM ac–ac converters," *IEEE Power Electron. Lett.*, vol. 1, no. 1, pp. 10–13, Mar. 2003.

[2] B. H. Kwon, B. D. Min, and J. H. Kim, "Novel topologies of AC choppers," *IEE Proc. Electr. Power Appl.*, vol. 143, no. 4, pp. 323–330, Jul. 1996.

[3] F. Z. Peng, "Revisit power conversion circuit topologies-recent advances and applications,"in *Proc. IEEE Int. Power Electr. Motion Conf.*, May 2009, pp. 188–192.

[4] L. M. Tolbert, F. Z. Peng, F. H. Khan, and S. Li, "Switching cells and their implications for power electronic circuits," in *Proc. IEEE Int. Power Electr. Motion Conf.*, 2009, pp. 773–779.

[5] F. H. Khan, L. M. Tolbert, and F. Z. Peng, "Deriving new topologies of DC–DC converters featuring basic switching cells," *Proc. IEEE Workshop Comput. Power Electron.*, 2006, pp. 328–332.

[6] J. Salmon, A. Knight, J. Ewanchuk, and N. Noor, "Multi-level single phase boost rectifiers using coupled inductors," *Proc. IEEE Int. Power Electr. Motion Conf.*, 2008, pp. 3156–3163.

[7] C. Chapelsky, J. Salmon, and A. M. Knight, "High-quality single-phase power conversion by reconsidering the magnetic components in the output stage-building a better half-bridge," *IEEE Trans. Ind. Appl.*, vol. 45, no. 6, pp. 2048–2055, Nov./Dec. 2009.

[8] J. Salmon, J. Ewanchuk, and A. Knight, "Single phase multi-level PWM inverter topologies using coupled inductor," in *Proc. IEEE Power Electron. Spec. Conf.*, Jun. 2008, pp. 802–808.

[9] J. Salmon, J. Ewanchuk, and A. M. Knight, "PWM inverters using split-wound coupled inductors," *IEEE Trans. Ind. Appl.*, vol. 45, no. 6, pp. 2001–2009, Nov./Dec. 2009.

[10] Z. Chenghua, Z. Fanghua, and Y. Yangguang, "A novel split phase dual buck half bridge inverter," *Proc. IEEE Appl. Power Electron. Conf. Expo.*, 2005, vol. 2, pp. 845–849.
[11] L. Chuang, S. Pengwei, L. Jih-Sheng, J. Yanchao, W. Mingyan, C. Chien-Liang, and C. Guowei, "Cascade dual-boost/buck active-front-end converter for intelligent universal transformer," *IEEE Trans. Ind. Electron*, vol. 59, no. 12, pp. 4671–4680, Dec. 2012.
[12] S. Pengwei, L. Chuang, L. Jih-Sheng, and C. Chien-Liang, "Cascade dual buck inverter with phase-shift control," *IEEE Trans. Power Electron.*, vol. 27, no. 4, pp. 2067–2077, Apr. 2012.
[13] S. Pengwei, L. Chuang, L. Jih-Sheng, C. Chien-Liang, and K. Nathan, "Three-phase dual-buck inverter with unified pulsewidth modulation," *IEEE Trans. Power Electron.*, vol. 27, no. 3, pp. 1159–1167, Mar. 2012.
[14] X. Zhang and C. Gong, "Dual-buck half-bridge voltage balancer," *IEEE Trans. Ind. Electron.*, vol. 60, no. 8, pp. 3157–3164, Aug. 2013.
[15] Y. Zhilei, X. Lan, and Y. Yangguang, "Control strategy for series and parallel output dual-buck half bridge inverters based on DSP control," *IEEE Trans. Power Electron.*, vol. 24, no. 2, pp. 434–444, Feb. 2009.
[16] Y. Zhilei, X. Lan, and Y. Yangguang, "Dual-buck full-bridge inverter with hysteresis current control," *IEEE Trans. Ind. Electron.*, vol. 56, no. 8, pp. 3153–3160, Aug. 2009.
[17] Y. Zhilei and X. Lan, "Two-switch dual-buck grid-connected inverter with hysteresis current control," *IEEE Trans. Power Electron.*, vol. 27, no. 7, pp. 3310–3318, Jul. 2012.
[18] N. R. Zargari, P. D. Ziogas, and G. Joos, "A two-switch high-performance current regulated DC/AC converter module," *IEEE Trans. Ind. Appl.*, vol. 31, no. 3, pp. 583–589, May/Jun. 1995.
[19] S. Hyunhak, C. Honnyong, K. Heung-Geun, and Y. Dong-Wook, "A novel single-phase PWM AC–AC converters without commutation problem," in *Proc. IEEE Energy Convers. Congr. Expo.*, 2013, pp. 2355–2362.
[20] S. Pengwei, L. Chuang, L. Jih-Sheng, and C. Chien-Liang, "Grid-tie control of cascade dual-buck inverter with wide-range power flow capability for renewable energy applications," *IEEE Trans. Power Electron.*, vol. 27, no. 4, pp. 1839–1849, Apr. 2012.

Hyun-Hak Shin received the B.S. degree in electrical engineering from Yeungnam University, Gyeongsangbuk-do, Korea, in 2012. He is currently working toward the master's degree in the School of Energy Engineering, Kyungpook National University, Daegu, Korea.

His current research interests include a novel PWM ac–ac converters, Z-source inverters, and solid-state transformer (SST).

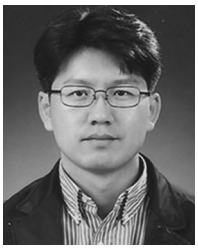

Honnyong Cha (S'08–M'10) received the B.S. and M.S. degrees in electronics engineering from Kyungpook National University, Daegu, Korea, in 1999 and 2001, respectively, and the Ph.D. degree in electrical engineering from Michigan State University, East Lansing, MI, USA, in 2009.

From 2001 to 2003, he was a Research Engineer with the Power System Technology Company, An-san, Korea. From 2010 to 2011, he worked as a Senior Researcher at the Korea Electrotechnology Research Institute, Changwon, Korea. In 2011, he joined the Kyungpook National University as an Assistant Professor in the School of Energy Engineering. His current research interests include high power dc–dc converters, dc–ac inverters, Z-source inverters, and power conversion for electric vehicles and wind power generation.

Heung-Geun Kim (S'82–M'88–SM'12) was born in Korea, in 1956. He received the B.S., M.S., and Ph.D. degrees in electrical engineering from Seoul National University, Seoul, Korea, in 1980, 1982, and 1988, respectively.

Since 1984, he has been with the Department of Electrical Engineering, Kyungpook National University, Daegu, Korea, where he is currently a Full Professor and the Director of the Microgrid Research Center. He was a Visiting Scholar at the Department of Electrical and Computer Engineering, University of Wisconsin-Madison, Madison, WI, USA, from 1990 to 1991, and at the Department of Electrical Engineering, Michigan State University, East Lansing, MI, USA, from 2006 to 2007. His current research interests include ac machine control, PV power generation, and microgrid system.

Dong-Wook Yoo (M'90) received the B.S. degree in electrical engineering from Sung-Kyun-Kwan University (SKKU), Suwon, Korea, in 1983, the M.S. degree in electrical engineering from Yon-Sei University, Seoul, Korea, in 1985, and the Ph.D. degree from SKKU in 1997.

Since 1985, he has been working at Korea Electrotechnology Research Institute (KERI), Changwon, Korea, as a Researcher, Senior Researcher, and Principal Researcher. He is currently the Head of Power Conversion and Control Laboratory, and HVDC Research Division at KERI. He is the author and coauthor of more than 30 publications in IEEE TRANSACTIONS, and the holder of more than 60 Korean patents, including six U.S. patents.

Dr. Yoo is a Member of the IEEE Power Electronics Specialists Conference and the IEEE Industrial Applications Conference, the Korean Institute of Power Electronics (KIPE), and the Korean Institute of Electrical Engineers (KIEE). Since 1999, he has been a Committee Member of KIPE, from 2009 to 2010, a Committee Member of KIEE, from 2005 to 2006 and 2009, served as the Chairman of the KIPE conference, and the Vice President of KIPE from 2010 to 2011. He was the co-recipient of the 2002 IEEE IECON Best Paper Award, the 2007 ICPE Best Paper Award, the 2011 KIPE JPE Best Paper Award, and the 2013 KERI Grand Award.